Characterizing weak chaos using time series of Lyapunov exponents

R. M. da Silva,[1] C. Manchein,[1] M. W. Beims,[2,3] and E. G. Altmann[3]
[1]*Departamento de Física, Universidade do Estado de Santa Catarina, 89219-710 Joinville, Brazil*
[2]*Departamento de Física, Universidade Federal do Paraná, 81531-980 Curitiba, Brazil*
[3]*Max-Planck-Institute for the Physics of Complex Systems, Nöthnitzer Str. 38, 01187, Dresden, Germany*
(Received 28 October 2014; published 8 June 2015)

We investigate chaos in mixed-phase-space Hamiltonian systems using time series of the finite-time Lyapunov exponents. The methodology we propose uses the number of Lyapunov exponents close to zero to define regimes of ordered (stickiness), semiordered (or semichaotic), and strongly chaotic motion. The dynamics is then investigated looking at the consecutive time spent in each regime, the transition between different regimes, and the regions in the phase space associated to them. Applying our methodology to a chain of coupled standard maps we obtain (i) that it allows for an improved numerical characterization of stickiness in high-dimensional Hamiltonian systems, when compared to the previous analyses based on the distribution of recurrence times; (ii) that the transition probabilities between different regimes are determined by the phase-space volume associated to the corresponding regions; and (iii) the dependence of the Lyapunov exponents with the coupling strength.

DOI: 10.1103/PhysRevE.91.062907 PACS number(s): 05.45.Ac, 05.45.Pq

I. INTRODUCTION

In weakly chaotic Hamiltonian systems regions of regular (periodic and quasiperiodic) and chaotic motion typically coexist in the phase space [1,2]. In high dimensions, due to Arnold diffusion, all initial conditions leading to chaotic motion are connected in the phase space building a single chaotic component [1]. Even if the volume of the regular regions becomes vanishingly small, as expected for high-dimensional nonlinear systems, the dynamics inside the chaotic component of the phase space is strongly affected by such regions. This happens because trajectories approaching nonhyperbolic regions or regular motion remain close to them a long time before visiting again other parts of the chaotic component of the phase space. This signature of weak mixing (or weak chaos) is known as stickiness [3–8].

Since the work in Ref. [3], the main quantification of stickiness in Hamiltonian systems has been through the fat-tail distribution of Poincaré recurrence times (see, e.g., Refs. [4,8,9]). An alternative approach is to use finite-time Lyapunov exponents (FTLEs) [10–12], with recent applications using large deviation techniques [7,13] and the cumulants [14,15] of the FTLE distribution. In area-preserving maps, stickiness generically occurs at the border of two-dimensional Kolmogorov-Arnold-Moser (KAM) island [1] (i.e., at one-dimensional tori). The recurrence time is a measure of the time the trajectory spends around such structures before returning to the chaotic sea (stickiness happens also to one-parameter families of parabolic orbits [16,17] and even to isolated parabolic fixed points [4,18,19]). Near the nonhyperbolic structures, the local instability of chaotic trajectories is reduced so that FTLEs can be used to characterize phase-space regions of interest [11–13,20,21]. Stickiness has also been studied in higher-dimensional systems [9,10,14,15,21,22], and long recurrence times can be due to different nonhyperbolic regions and tori of different dimensionalities [23]. An improved characterization of stickiness events (long recurrence time) thus requires us to measure the number of stable and unstable directions in the trajectory during this event. Froeschlé conjectured that lower-dimensional tori could not exist [1,24,25]. In early studies in the 1980s such events of stickiness to lower-dimensional tori were reported in some systems [21] but were not found in other examples [10]. Even if invariant tori do not exist, a small local Lyapunov exponent could effectively act as a lower-dimensional trap. This is similar to almost invariant sets [26,27], which are regions in phase space where typical trajectories stay (on average) for long periods of time.

In this paper we introduce a methodology that uses time series of local Lyapunov exponents to define regimes of ordered, semiordered, and totally chaotic motion and obtain an improved characterization of stickiness in high-dimensional Hamiltonian systems. We illustrate this general procedure in a chain of coupled standard maps and confirm that stickiness events of different times length are dominated by trajectories with different FTLEs. A significant improvement of the characterization of sticky motion in high-dimensional systems is found. We also characterize the FTLEs for small couplings and compare them to expected universal properties in fully chaotic systems [28]. The method proposed here is general and can be used to investigate Hamiltonian systems in any dimension.

The paper is divided as follows. In Sec. II we describe the Hamiltonian model we use to illustrate our method. In Sec. III we introduce our method to compute and analyze time series of local Lyapunov exponents. This methodology is then applied to the symplectic model of coupled standard maps in Sec. IV. Section V summarizes the main results of the paper.

II. THE COUPLED MAPS MODEL

We use a time-discrete $2N$-dimensional Hamiltonian system obtained as the composition $\mathbf{T} \circ \mathbf{M}$ of independent one-step iteration of N symplectic two-dimensional maps $\mathbf{M} = (M_1, \ldots, M_N)$ and a symplectic coupling $\mathbf{T} = (T_1, \ldots, T_N)$. As a representative example of two-dimensional maps we choose for our numerical investigation the standard map:

$$\mathbf{M_i}\begin{pmatrix} p_i \\ x_i \end{pmatrix} = \begin{pmatrix} p_i + K_i \sin(2\pi x_i) & \mod 1 \\ x_i + p_i + K_i \sin(2\pi x_i) & \mod 1 \end{pmatrix}, \quad (1)$$

and for the coupling

$$\mathbf{T_i}\begin{pmatrix} p_i \\ x_i \end{pmatrix} = \begin{pmatrix} p_i + \sum_{j=1}^{N} \xi_{i,j} \sin[2\pi(x_i - x_j)] \\ x_i \end{pmatrix}, \quad (2)$$

with $\xi_{i,j} = \xi_{j,i} = \frac{\xi}{\sqrt{N-1}}$ (all-to-all coupling). The motivation for working with this system is that in the limit of small coupling $\xi \to 0$ it can be understood looking at the dynamics of the N uncoupled maps. This system was studied in Refs. [6,9] using recurrence time distribution. This allow us to critically compare the benefits of our methodology. In all numerical simulations we used $K_1 = 0.5214$ for the map M_1 and $K_2 = K_3 = 0.5108$ for the maps M_2 and M_3.

III. METHOD

In this section we describe the method proposed in this work. To be illustrative, we present numerical simulations for the system defined in Sec. II.

A. Lyapunov spectrum and the classification of ordered, semiordered or semichaotic, and chaotic regimes

Consider a chaotic trajectory in a closed Hamiltonian system which, after reducing the phase-space dimension due to global invariant of motion, has N degrees of freedom. For long times t the trajectory ergodically fills the whole chaotic component of the phase space, which is characterized by a spectrum of N Lyapunov exponents $\{\lambda_{i=1\ldots N}^{(\infty)}\}$, where $\lambda_1^{(\infty)} > \lambda_2^{(\infty)}, \ldots, \lambda_N^{(\infty)} > 0$ [29]. The central ingredient of our analysis is the spectrum of FTLEs computed along a trajectory during a window of size ω where we obtain a time-dependent spectrum $\{\lambda_i^{(\omega)}\}(t) = \{\lambda_i^{(\omega)}\}$. The window size ω has to be sufficiently small to guarantee a good resolution of the temporal variation of the $\lambda_i^{(\omega)}$, but sufficiently large in order to have a reliable estimation (see Refs. [10–12]). The probability density function of $\lambda_i^{(\omega)}$ has been extensively studied [7,10–12]. Here we go beyond the study of the probability density function and explore temporal properties in the time series of $\{\lambda_i^{(\omega)}\}$.

Figures 1(a) and 1(b), for $N = 2$ and 3, respectively, show the time series of $\lambda_i^{(\omega)}$ $(i = 1, \ldots, N)$. The sharp transitions towards $\lambda_i^{(\omega)} \approx 0$ motivate the classification in regimes of motion [20,21] as (a) *ordered* ($\lambda_{1,2}^{(\omega)} \approx 0$), (b) *semiordered or semichaotic* ($\lambda_1^{(\omega)} > 0; \lambda_2^{(\omega)} \approx 0$), and (c) *chaotic* ($\lambda_{1,2}^{(\omega)} > 0$). For a system with N degrees of freedom we will say that the trajectory is in a regime of type $S_M^{(N)}$ if it has M local Lyapunov exponents $\lambda_i^{(\omega)} > \varepsilon_i$, where $\varepsilon_i \ll \lambda_i^{(\infty)}$ are the small thresholds. This means that $S_0^{(N)}$ and $S_N^{(N)}$ are ordered and chaotic regimes, respectively. Whenever there is no ambiguity, we will drop the superscript $S_M^{(N)} = S_M$ to have a simpler notation.

Practical implementations of the general method described above require the choice of a few parameters and conventions. First, the window size ω and the threshold ε_i directly affect the classification in regimes. They can be thought of as the phase-space resolution of the analysis and should be chosen so that they provide maximal information about the regions of interest. Unless stated otherwise, we use $\omega = 100$ and $\varepsilon_i \approx 0.10\langle\lambda_i^{(\omega)}\rangle$, where $\langle\ldots\rangle$ denotes average over t, where $t = 1, \ldots, t_L$ (even though the *classification* in regimes is strongly ω-dependent, our *conclusions* are not sensitively affected by variations around the chosen values). Another important choice is the method for computation of the FTLEs. We use Benettin's algorithm [30,31], which includes the Gram-Schmidt reorthonormalization procedure. The decreasing order of $\lambda_i^{(\omega)}$ is valid on average, but inversions of the order $(\lambda_{i+1}^{(\omega)} > \lambda_i^{(\omega)})$ may happen for some times t, and we have chosen to impose the order of $\lambda_i^{(\omega)}$ for all t. Finally, it is possible to decide how to sample the time series $\lambda_i^{(\omega)}$. While the FTLEs are defined for all t, there is a trivial correlation between the values of FTLEs inside a window of size ω because they are computed using the same points of the trajectory. In order to avoid this trivial correlation, the series of $\lambda_i^{(\omega)}$ can be computed using nonoverlapping windows, i.e., plotting $\lambda_i^{(\omega)}$ only every ω time steps (a choice we adopt in our simulations).

B. Identifying phase-space regions

In order to understand the properties of the time series $\{\lambda_i^{(\omega)}\}$ it is useful to consider the phase-space regions associated to each regime S_M. We denote by $\mu(A)$ the phase-space volume (Liouville measure) of region A in the bounded phase space Γ, i.e., $\mu(\Gamma) \equiv 1$. The most important distinction is between the regions of regular Γ_{regular} and chaotic Γ_{chaos} motion. In Hamiltonian systems, typically $\mu(\Gamma_{\text{chaos}}) > 0$ and $\mu(\Gamma_{\text{regular}}) > 0$. In principle, the regular region Γ_{regular} can be subdivided according to the dimensionality of the tori. However, according to Froeschlé's conjecture, in a $2N$-dimensional phase space, tori with dimension N have positive measure and thus $\mu(\Gamma_{\text{regular}}) = \mu(\Gamma_{\text{tori}})$ [1,24,25]. For $N > 1$, the chaotic region Γ_{chaos} is expected to build a single ergodic component because tori of N dimension do not partition the $2N$-dimensional phase space in different regions, and therefore any chaotic trajectories eventually explores (through Arnold diffusion) the whole Γ_{chaos}. Our interest is not to test the Froeschlé conjecture or Arnold diffusion, but to show the insights about the chaotic dynamics we can obtain using the time series of $\{\lambda_i^{(\omega)}\}$ together with the definition of the regimes S_M. One application is to use the regimes S_M to split the chaotic component of the phase space in meaningful components. This is done by considering the set of points $\boldsymbol{X}_M^{(N)}$ in the phase space leading to each regime S_M as

$$\boldsymbol{X}_M^{(N)} = \lim_{t_L \to \infty} \boldsymbol{x}_t(\boldsymbol{x}_t \in S_M), \quad (3)$$

where t_L is the total length of the trajectory and $\boldsymbol{x}_t \in S_M$ indicates that at time t the trajectory at $\boldsymbol{x}_t$ had $\{\lambda_i^{(\omega)}\} \in S_M$.

Figure 2 shows numerical estimates of the phase-space regions obtained for each regime S_M in the chain of coupled maps defined in Sec. II. The regime S_0 (or the ordered regime) is associated to the region localized close to the border of the KAM island of the uncoupled case [compare to Fig. 2(a)]. Points which belong to the regime S_1 are close to the center of the torus from the uncoupled case. This suggests that when trajectories are inside the region related to regime S_1, they more likely penetrate inside the torus from the uncoupled case. In the chaotic sea both regimes S_1 and S_2 are visible. These results are naturally understood in the perturbative limit (small coupling $\xi \ll 1$). The regime S_0 corresponds to $\lambda_i^{(100)} \approx 0$ for

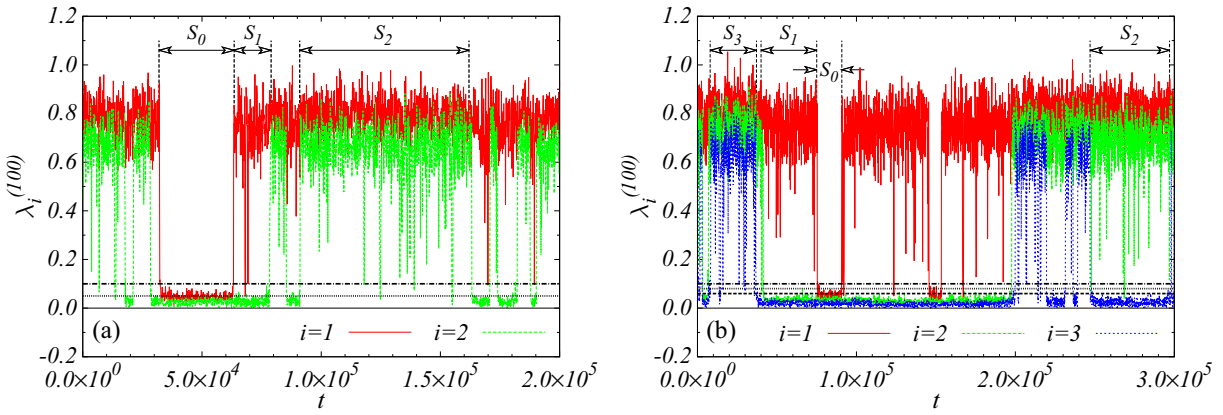

FIG. 1. (Color online) Illustration of the method proposed to define the regimes S_M. Time series of the spectrum of FTLEs $\{\lambda_i^{(\omega=100)}\}$, with $i = 1,\ldots,N$, for the map (1)–(2) with $\xi = 10^{-3}$. (a) Case $N = 2$ and the thresholds $\varepsilon_1 = 0.1$ and $\varepsilon_2 = 0.05$ are represented by dash-dotted and dotted lines, respectively. (b) Case $N = 3$ and the thresholds $\varepsilon_1 = 0.1$, $\varepsilon_2 = 0.08$, and $\varepsilon_3 = 0.06$ are represented by dash-dotted, dotted, and dashed lines, respectively.

every $i = 1,\ldots,N$, which is expected when the trajectory is stuck close to the N-dimensional tori built as the product of the one-dimensional tori of the uncoupled maps. In contrast, S_M for $M > 0$ implies that at least one FTLE $\lambda_i^{(\omega)} \gg 0$ and therefore the trajectory projected in one map can be both in the chaotic and regular regions (e.g., S_1 for $N = 2$ can be obtained from $\lambda_1^{(\omega)} \gg 0, \lambda_2^{(\omega)} \approx 0$ or from $\lambda_1^{(\omega)} \approx 0, \lambda_2^{(\omega)} \gg 0$). Altogether, these observations confirm that our method allows for a meaningful division of the chaotic component of the phase space and can thus be used to identify regions of interesting dynamics. In the case where partial barriers exist inside the chaotic component, such as in area-preserving maps with mixed phase space [2], we expect the regions obtained through our method to depend weakly on ω and to coincide with those obtained from the partial barriers.

IV. RESULTS

In this section we apply the Lyapunov time-series methodology described in Sec. III to the $2N$-dimensional system defined in Sec. II. We compute and interpret four basic properties of the method: the total time spent in each regime (residence time), the transition between regimes, the consecutive time in each regime, and the scaling of Lyapunov exponents.

A. Residence time in each regime

The first and most basic quantity we measure is the probability $P(S_M)$ of finding the trajectory in each regime, defined as the fraction of the total time t_L that $\boldsymbol{x}_t \in S_M$ (i.e., $P(S_M) = \sum_{t=0}^{t_L} \delta_{t\in S_M}/t_L$, where $\delta_{t\in S_M} = 1$ if $t \in S_M$ and $\delta_{t\in S_M} = 0$ otherwise).

Figure 3 shows the probabilities $P(S_M)$ for the map with $N = 2,3$ as a function of the coupling strength ξ. We now explain the behavior of $P(S_M)$ with ξ by discussing the effect of coupling ξ on the phase-space regions associated to S_M, as defined in Sec. III B. By the ergodicity of Γ_{chaos}, $P(S_M)$ corresponds to the (normalized) volume of the region related to regime S_M in the phase space

$$P(S_M) = \frac{\mu(S_M)}{\mu(\Gamma_{\text{chaos}})} = \frac{\mu(S_M)}{1-\mu(\Gamma_{\text{tori}})}. \tag{4}$$

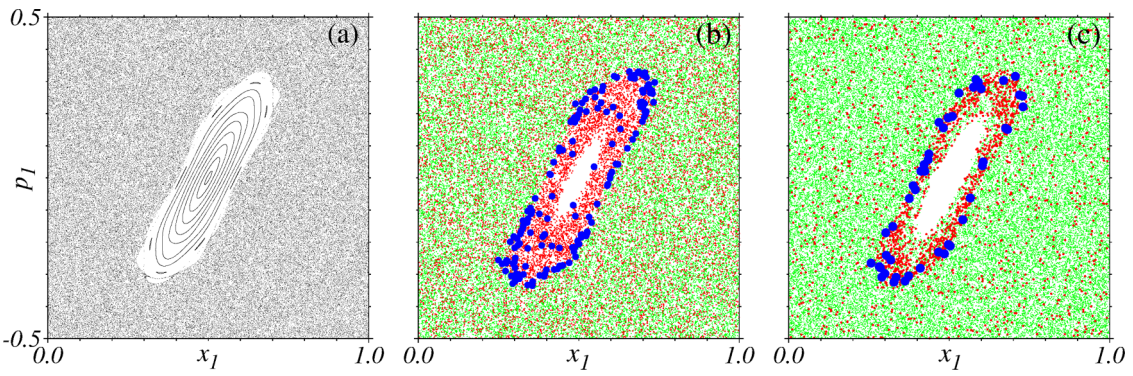

FIG. 2. (Color online) Phase space projected in (x_1, p_1) for different configuration of the N-coupled standard maps defined in Sec. II. (a) $N = 1$ (uncoupled case), showing 10^2 randomly started initial conditions and plotting as dots 10^4 iterations of each of them. A large KAM island can be seen at the center of the plot; (b) $N = 2$ and coupling strength $\xi = 10^{-3}$; (c) $N = 3$ and $\xi = 10^{-3}$. Symbols with different colors in panels (b, c) show points $\boldsymbol{x}_t \in S_M$ belonging to regimes S_0 (blue circles), S_1 (red points), and S_2 (green points). These points were computed starting a single trajectory in the chaotic region of all maps and iterating it 5×10^6 times.

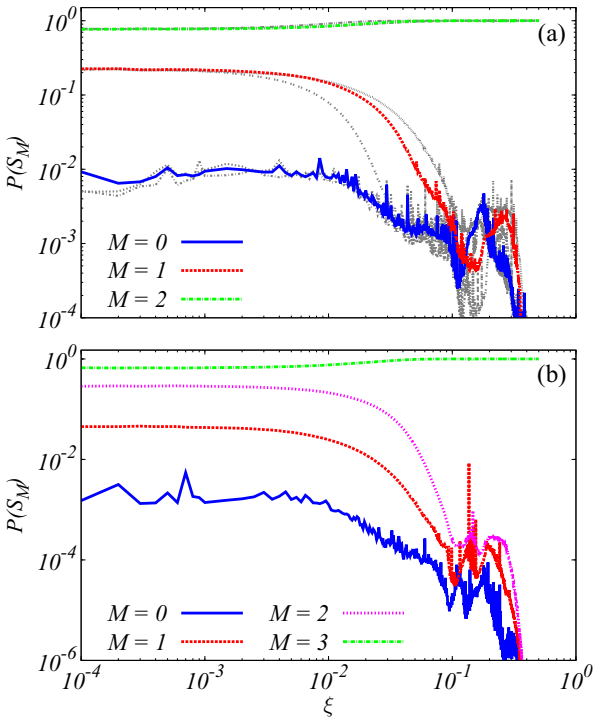

FIG. 3. (Color online) Residence time in each regime S_M. (a) $N = 2$ with $\varepsilon_1 = 0.1$ and $\varepsilon_2 = 0.05$. (b) $N = 3$ with $\varepsilon_1 = 0.1$, $\varepsilon_2 = 0.08$, and $\varepsilon_3 = 0.06$. In panel (a) the values obtained with $\omega = 100$ are compared with results for $\omega = 50$ and $\omega = 500$ (gray curves). Only for the case $M = 1$ do the gray curves (right for $\omega = 50$ and left for $\omega = 500$) show a shift in the x axis ξ. Estimations for each ξ are based on a trajectory with length $t_L = 10^{10}$.

The results of Fig. 3 show that the chaotic region is the largest region in phase space for any coupling, while the region associated to S_1 has a larger volume than S_0 for couplings $\xi \lesssim 1.3 \times 10^{-1}$. For larger ξ we see oscillations with a local maximum close to $\xi \sim 2 \times 10^{-1}$ for the cases $M = 0$ and $M = 1$.

We now interpret the ξ dependence observed in Fig. 3 by arguing how the different terms in Eq. (4) vary with ξ. We denote by $\mu(U_j)$ the measure of tori for the jth map with control parameter K_j in the uncoupled case $\xi = 0$ (which we assume to be approximately equal to the measure of the KAM islands). For small coupling $\xi \approx 0$ we expect that most tori of the uncoupled maps to survive and therefore:

(i) $\mu(\Gamma_{\text{tori}}) \approx \prod_{j=1}^{N} \mu(U_j)$, which in the simple case of $\mu(U_j) = \mu$ for all j reduces to $\mu(\Gamma_{\text{tori}}) \approx \mu^N$. (ii) $\mu(S_{M=0})$ corresponds to a small volume around Γ_{tori}, i.e., $\mu(S_{M=0}) \sim \mu(\Gamma_{\text{tori}}) \approx P(S_0)/[1 + P(S_0)]$. (iii) For $\mu(S_{M\neq 0})$ we have that $N - M$ maps are in their corresponding KAM island (with probability $\mu(U_j)$) and M maps in the chaotic area [with probability $1 - \mu(U_k)$]. For example, for $N = 3$ and $M = 2$ we have that

$$\begin{aligned}\mu(S_{M=2}) = {} & \mu(U_1)[1-\mu(U_2)][1-\mu(U_3)] \\ & + \mu(U_2)[1-\mu(U_1)][1-\mu(U_3)] \\ & + \mu(U_3)[1-\mu(U_1)][1-\mu(U_2)].\end{aligned}$$

In general this leads to

$$\mu(S_M) \approx \sum_{j_1} \cdots \sum_{j_M} \prod_{j\in\{j_1,\ldots,j_M\}} (1-\mu_j) \prod_{j\notin\{j_1,\ldots,j_M\}} \mu_j,$$

where the last product is over all $j = 1, \ldots, N$ except $j \in \{j_1, \ldots, j_M\}$. In the simple case of $\mu(U_j) = \mu$, it reduces to $\mu(S_M) \approx \binom{N}{M} \mu^{N-M}(1-\mu)^M$.

We now consider the effect of growing ξ. In the spirit of the KAM theorem, the tori of the coupled maps (generated as the product of the N maps) are expected to be robust to small couplings ξ, which act as a perturbation. This explains why the curves in Fig. 3 are essentially flat for small ξ. Increasing ξ even further, the nonlinearity of the system increases, and therefore $\mu(\Gamma_{\text{tori}})$ is expected to decrease [$\mu(\Gamma_{\text{tori}}) \to 0$ for $\xi \gg 0$]. This reduction of the tori leads to an increase in the denominator of Eq. (4) and explains the observed tendency of reduction of $P(S_M)$ for all regions related to stickiness ($M < N$). Indeed, for $\xi > 0.5$ no signature of tori or stickiness was detected numerically and $P(S_{M=N}) = 1$. The nontrivial dependencies of $P(S_{M<N})$ in Fig. 3 appear at $\xi \sim 2 \times 10^{-1}$ values, close to the values of ξ for which the last tori disappear (see also Fig. 7.2 in Ref. [6]). In this regime the volume of the tori is already negligible $\mu(\Gamma_{\text{tori}}) \gtrsim 0$, but stickiness is still effective (notice that even zero measure nonhyperbolic sets can lead to stickiness [7,17]). The denominator in Eq. (4) is therefore $1 - \mu(\Gamma_{\text{tori}}) \sim 1$, not significantly affected by further increases of ξ, and therefore not driving the reduction of $P(S_{M<N})$. Small variations of a control parameter of the system (in this case ξ) are known to lead to sensitive creation and destruction of tori, with nontrivial dependencies on the stickiness [5]. We can thus expect that, close to the disappearance of the tori, the small volume of stickiness regions $\mu(S_{M<N})$ fluctuate with ξ leading even to an increase with ξ. It is interesting to note that this nontrivial increase with ξ appears for $P(S_{M=0})$ in Fig. 3 precisely when the curves $P(S_{0<M<N})$ show a sharp decreasing fluctuation. This suggests an exchange between measure of different sticky regions associated to regimes $S_{M<N}$, without interference of the much larger fully chaotic component $S_{M=N}$.

B. Transitions between regimes

We now focus on the transition between regimes. The simplest analysis correspond to the two-time (joint) probability $P(S_M \to S_{M'})$, computed as the fraction of the total trajectory time t_L that $\boldsymbol{x}_t \in S_M$ and $\boldsymbol{x}_{t+1} \in S_{M'}$. The probabilities considered in the previous section can be obtained as $\sum_{S_M} P(S_M \to S_{M'}) = P(S_{M'})$ and $\sum_{S_{M'}} P(S_M \to S_{M'}) = P(S_M)$. Figure 4(a) shows the dependence of $P(S_M \to S_{M'})$ on ξ for our model. We notice that $P(S_M \to S_{M'})$ is equal to $P(S_{M'} \to S_M)$. This is expected considering that the system is ergodic, volume preserving, and time reversible. The dependence of $P(S_M \to S_{M'})$ on ξ follows a similar pattern observed for $P(S_M)$ in Fig. 3. More information is obtained from the conditional probability

$$P_{M,M'} \equiv P(S_M \to S_{M'}|S_M) \equiv \frac{P(S_M \to S_{M'})}{P(S_M)}, \qquad (5)$$

which quantifies the probability that trajectories at S_M will move to $S_{M'}$. The results shown in Fig. 4(b)–(d) show for all

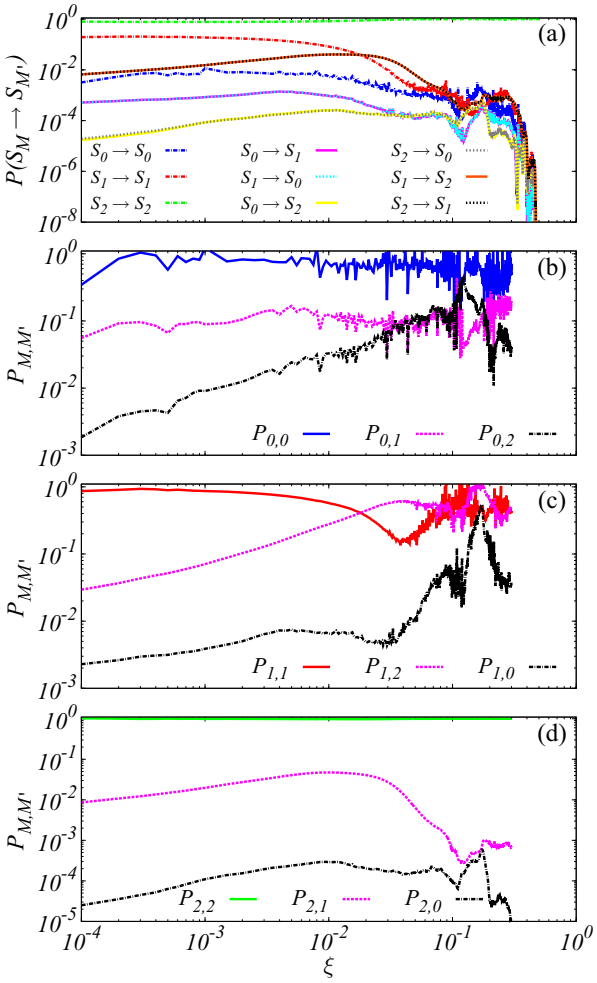

FIG. 4. (Color online) Transition between regimes S_M as a function of the coupling strength ξ. (a) Transition probability $P(S_M \to S_{M'})$; (b)–(d) conditional probability $P_{M,M'}$ defined in Eq. (5) of moving to M' given that the trajectory was at M. Estimations for each ξ based on a single trajectory with length $t_L = 10^{10}$ in the case of $N = 2$ coupled maps and $\varepsilon_1 = 0.1$ and $\varepsilon_2 = 0.05$.

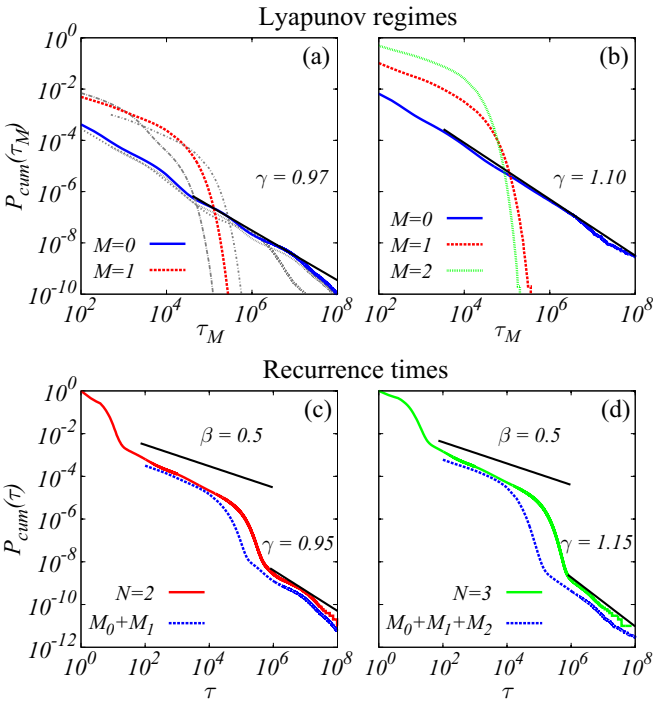

FIG. 5. (Color online) Comparison between our method and the analysis based on recurrence time. The cumulative distribution $P_{\rm cum}(\tau_M)$ of times τ_M is shown for each regime $S_{M<N}$ for $\omega = 100$ and (a) $N = 2$ and (b) $N = 3$. In panel (a) the gray curves show results for $\omega = 50$ and $\omega = 500$. Only for the case $M = 1$ do the gray curves (left for $\omega = 50$ and right for $\omega = 500$) show a shift in the x axis ξ. The cumulative distribution $P_{\rm cum}(\tau)$ for recurrence times τ to a region in the chaotic component of the phase space (in $S_{M=N}$) for (c) $N = 2$ and (d) $N = 3$. For comparison, in panel (c) we show the results obtained combining the normalized curves for $M_0 + M_1$ (blue dotted line: divided by 1.7×10^3 for convenience of scale) of panel (a), and in panel (d) the normalized curves for $M_0 + M_1 + M_2$ (blue dotted line: divided by 10^3) of panel (b). Results obtained using maps of Sec. II with $\xi = 10^{-3}$, $\varepsilon_1 = 0.1$ and $\varepsilon_2 = 0.05$ for the case $N = 2$ and $\varepsilon_1 = 0.1$, $\varepsilon_2 = 0.08$ and $\varepsilon_3 = 0.06$ for the case $N = 3$.

S_M that (i) persistence in the same S_M $[P(S_M \leftrightarrow S_M|S_M)]$ is dominant and (ii) the most likely transitions occur between neighboring regimes (e.g., $P_{2,1} > P_{2,0}$). The only (slight) deviations of this picture happen for large values of ξ, close to the disappearance of the KAM island. Altogether, these results confirm that in the perturbative regime ($\xi \ll 1$) stickiness happens approaching the region of regular motion of different maps one after the other (in opposite to a direct approach from S_0 to $S_{M=N}$).

C. Consecutive time in each regime

The results of the previous section confirm that residence in the same regime is the dominant behavior. This motivates us to study the time τ_M spent consecutively in a regime S_M (i.e., τ_M is the time between two consecutive transitions between different regimes, the first to S_M and the second out of S_M). In a trajectory of length t_L we collect a series of τ_M. We are mainly interested in the probability distribution $P(\tau_M)$ [or equivalently its cumulative $P_{\rm cum} \equiv \sum_{\tau'_M=\tau_M}^{\infty} P(\tau'_M)$] for different S_M in the limit $t_L \to \infty$. These distributions should be compared to the distribution of recurrence times τ, defined as the time between two successive entries to a predefined recurrence region (usually taken in the fully chaotic component of the phase space). Events in the tails of $P(\tau)$ are associated to times for which the trajectory is stuck to the nonhyperbolic components of the phase space and $P(\tau)$ is the traditional method to quantify stickiness in Hamiltonian systems [3,4,8,9].

The numerical simulations in Fig. 5 confirm that the distribution obtained summing $P_{\rm cum}(\tau_M)$ for ordered and semiordered regimes (or $S_{M<N}$) is equivalent to cumulative distribution $P_{\rm cum}(\tau)$ obtained using recurrences. This is in agreement with the association of long consecutive times in regimes of ordered and semiordered motion to long recurrence times. Looking at the individual distributions $P_{\rm cum}(\tau_M)$ provide valuable additional information on the sticky motion. For semiordered motion (when $0 < M < N$) we observe an exponential tail after an intermediate decay with scaling $\beta \approx 0.5$. This behavior confirms the interpretation given in Ref. [9].

More interestingly, the $M = 0$ case shows an asymptotic algebraic decay which characterize stickiness. While the scaling is compatible with the results obtained using recurrence time, $P_{\rm cum}(\tau_{M=0})$ obtained in our methodology provides a better characterization of the scaling (over several orders of magnitudes) and allows for an independent analysis of the different regimes. These properties are essential when dealing with high-dimensional systems (which may contain different preasymptotic regimes) and for an accurate estimation of the stickiness exponent γ. Finally, Fig. 5(a) shows that all decays discussed above remain (qualitatively) the same for different choices of ω, with the curve for $M = 1$ showing the largest sensitivity on ω [as in Fig. 3(a)].

D. Scaling of Lyapunov exponents

So far we have focused on the temporal properties of the time series of FTLEs $\lambda_i^{(\omega)}$ and how they change with the coupling strength ξ. We now consider how the values of the Lyapunov exponents respond to an external perturbation, which in our case is the coupling to the other maps. It is known that the largest exponent $\lambda_1^{(\infty)}$ is extremely sensitive to perturbation. More specifically, Daido's relation [28,32] states that for small couplings ξ to another chaotic system, a universal logarithmic singularity is observed,

$$\lambda_i^{(\omega\to\infty)} - \Lambda_i^{(\omega\to\infty)} \approx \frac{c}{|\ln(\xi)|}, \tag{6}$$

where $\Lambda_i^{(\omega\to\infty)}$ are the unperturbed Lyapunov exponents, c is a constant, and $i = 1,\ldots,N$. This relation is valid for totally chaotic systems and for small mismatches between Lyapunov exponents of the uncoupled systems compared to their fluctuations [32]. Here we investigate the relation $\lambda_i^{(\omega)} - \Lambda_i^{(\omega)}$ as a function of ξ, for distinct values of ω and different regimes S_M. To this end we compute the temporal averages of the FTLEs $\langle\lambda_i^{(\omega)}\rangle$ for times t such that $\{\lambda_i^{(\omega)}\} \in S_M$.

Our numerical simulations reported in Fig. 6 show that small values of ω lead to a situation in which $\langle\lambda_i^{(\omega)}\rangle \approx \langle\Lambda_i^{(\omega)}\rangle$ at a finite value of ξ [Figs. 6(a) and 6(b)], while larger values of ω lead to situations in which $\langle\lambda_i^{(\omega)}\rangle \neq \langle\Lambda_i^{(\omega)}\rangle$ for any ξ. These results depend crucially on our choice to impose the order of $\lambda_i^{(\omega)}$ for all t, as discussed in Sec. III A. This makes the average over the trajectory time $\langle\lambda_i^{(\omega)}\rangle$ to be ω-dependent and different from the average over the Lyapunov time $\lambda_i^{(\omega\to\infty)}$. Applying the analysis without the division in regimes S_M leads to strongly fluctuating results [Figs. 6(a), 6(c), and 6(e)]. Much smoother results [Figs. 6(b), 6(d), and 6(f)] are obtained when we apply our method and compute $\langle\lambda_i^{(\omega)}\rangle$ only for t in the fully chaotic regime S_N. Looking at these smoother results we observe that the difference in Lyapunov exponents scales as $1/|\ln\xi|$, but that even for $\omega \to \infty$ the sticky motion leads to a deviation from Daido's relation (6) (curves are shifted vertically).

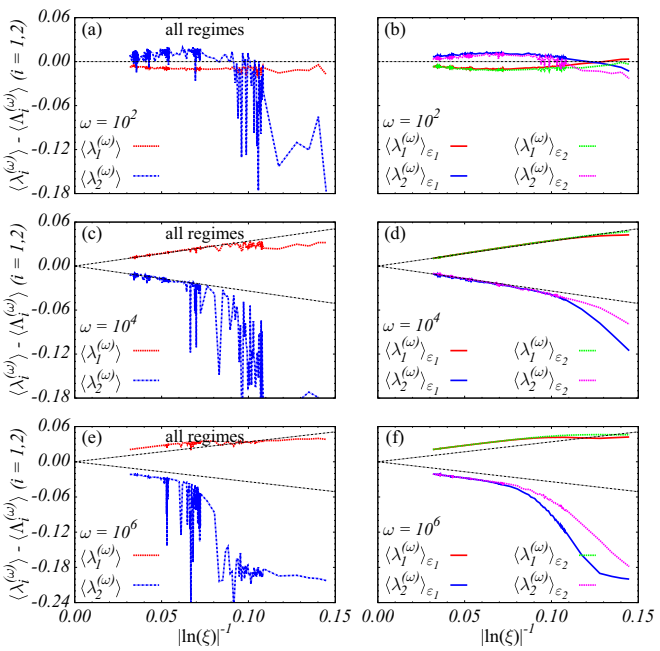

FIG. 6. (Color online) Sensitivity of the FTLEs for small couplings. The difference between the finite-time Lyapunov exponent in the coupled ($\langle\lambda_i^{(\omega)}\rangle$) and uncoupled ($\langle\Lambda_i^{(\omega)}\rangle$) maps as a function of $|\ln(\xi)|^{-1}$, where ξ is the coupling strength. Results are shown for $N = 2$ ($i = 1,2$) and different time windows ω (a)–(b) 10^2, (c)–(d) 10^4, and (e)–(f) 10^6. Black dashed lines in panels (c)–(f) are the expected linear behaviour, consistent with Eq. (6). Panels in the left column [(a), (c), and (e)] were computed for the full time series, while on the right column [(b), (d), and (f)] only FTLEs in the regime S_2 were used. The different colors correspond to different choices of threshold imposed to define the FTLE: $\langle\lambda_i^{(\omega)}\rangle_{\varepsilon_1}$ uses $\varepsilon_1 = 0.1\langle\lambda_i^{(\omega)}\rangle$ while $\langle\lambda_i^{(\omega)}\rangle_{\varepsilon_2}$ uses $\varepsilon_2 = 0.9\langle\lambda_i^{(\omega)}\rangle$, where $\langle\lambda_i^{(\omega)}\rangle$ is computed over the full time series (left column).

V. CONCLUSIONS

In summary, we have proposed a method to characterize the dynamics of Hamiltonian systems with mixed phase space based on time series of finite-time Lyapunov exponents. Using this method it is possible to define and study with high accuracy the time evolution of regimes of ordered, semiordered, and totally chaotic motion. This allows for an individualized characterization of the different stickiness mechanisms, improving alternative methods based on the statistics of recurrence times or on the distribution of finite-time Lyapunov exponents.

We applied our method to a chain of coupled standard maps and showed how the frequency of different regimes, and the transition probabilities between them, are related to the volume of different phase-space regions. Using the consecutive time in distinct regimes we have reproduced previous results obtained using recurrence times and showed that our method allows for a significant improvement in the characterization of the sticky motion (e.g., in the determination of the scaling exponents). This indicates that our method can be used to characterize stickiness in general high-dimensional systems and is particularly suited for cases in which different regions of sticky motion coexist. We have also shown that the dependence on the coupling strength of the largest Lyapunov exponents, after conveniently using our procedure, tend to follow only the qualitative universal properties of fully chaotic system.

Results obtained in a simple chain of standard maps confirm that our methodology can be applied to high-dimensional

systems and problems of current interest, such as controlling Fermi acceleration [33], galactic models [34], and plasma physics [35]. Another example of application is to associate each regime S_M with effective Hamiltonian functions, a procedure used to reproduce the complicated dynamics of kicking electrons [36] or the high harmonic generation in laser-assisted collisions [37].

ACKNOWLEDGMENTS

C.M. and R.M.S. thank CNPq, CAPES, and FAPESC, and M.W.B. thanks CNPq for financial support and MPIPKS in the framework of the Advanced Study Group on Optical Rare Events. C.M. also acknowledges the financial support and hospitality at the MPIPKS. E.G.A. thanks D. Pazó for suggesting the analysis performed in Sec. IV D.

[1] A. J. Lichtenberg and M. A. Lieberman, *Regular and Chaotic Dynamics* (Springer-Verlag, New York, 1992).
[2] J. D. Meiss, Rev. Mod. Phys. **64**, 795 (1992).
[3] B. V. Chirikov and D. L. Shepelyansky, Physica D **13**, 395 (1984).
[4] R. Artuso, Physica D **131**, 68 (1999).
[5] G. M. Zaslavsky, Phys. Rep. **371**, 461 (2002).
[6] E. G. Altmann, Ph.D. thesis, Max Planck Institut für Physik Komplexer Systeme, 2007.
[7] R. Artuso and C. Manchein, Phys. Rev. E **80**, 036210 (2009).
[8] G. Cristadoro and R. Ketzmerick, Phys. Rev. Lett. **100**, 184101 (2008).
[9] E. G. Altmann and H. Kantz, Europhys. Lett. **78**, 10008 (2007).
[10] H. Kantz and P. Grassberger, Phys. Lett. A **123**, 437 (1987).
[11] J. D. Szezech, S. R. Lopes, and R. L. Viana, Phys. Lett. A **335**, 394 (2005).
[12] M. Harle and U. Feudel, Chaos, Solitons Fractals **31**, 130 (2007).
[13] T. Laffargue, K.-D. N. T. Lam, J. Kurchan, and J. Tailleur, J. Phys. A: Math. Theor. **46**, 254002 (2013).
[14] C. Manchein, M. W. Beims, and J. M. Rost, Chaos **22**, 033137 (2012).
[15] C. Manchein, M. W. Beims, and J. M. Rost, Physica A **400**, 186 (2014).
[16] P. Gaspard and J. R. Dorfman, Phys. Rev. E **52**, 3525 (1995).
[17] E. G. Altmann, A. E. Motter, and H. Kantz, Phys. Rev. E **73**, 026207 (2006).
[18] R. Artuso and A. Prampolini, Phys. Lett. A **246**, 407 (1998).
[19] M. Sala, C. Manchein, and R. Artuso, arXiv:1410.4806.
[20] G. Contopoulos, L. Galgani, and A. Giorgilli, Phys. Rev. A **18**, 1183 (1978).
[21] A. Malagoli, G. Paladin, and A. Vulpiani, Phys. Rev. A **34**, 1550 (1986).
[22] D. Mingzhou, T. Bountis, and E. Ott, Phys. Lett. A **151**, 395 (1990).
[23] S. Lange, M. Richter, F. Onken, A. Bäcker, and R. Ketzmerick, Chaos **24**, 024409 (2014).
[24] C. Froeschlé, Astrophys. Space Sci. **14**, 110 (1971).
[25] C. Froeschlé, Astron. Astrophys. **16**, 172 (1972).
[26] M. Dellnitz and O. Junge, Int. J. Bif. Chaos **7**, 2475 (1997).
[27] G. Froyland and K. Padberg, Physica D **238**, 1507 (2009).
[28] H. Daido, Prog. Theor. Phys. **72**, 853 (1984).
[29] Without loss of generality we focus on the N largest Lyapunov exponents because due to the symplectic character of Hamiltonian systems the other N exponents are simply $\lambda_{N+1} = -\lambda_N, \lambda_{N+2} = -\lambda_{N-1}, \ldots \lambda_{2N} = -\lambda_1$.
[30] G. Benettin, L. Galgani, A. Giorgilli, and J.-M. Strelcyn, Meccanica **15**, 9 (1980).
[31] A. Wolf, J. B. Swift, H. L. Swinney, and J. A. Vastano, Physica D **16**, 285 (1985).
[32] R. Zillmer, V. Ahlers, and A. Pikovsky, Phys. Rev. E **61**, 332 (2000).
[33] A. L. P. Livorati, T. Kroetz, C. P. Dettmann, I. L. Caldas, and E. D. Leonel, Phys. Rev. E **86**, 036203 (2012).
[34] G. Contopoulos and M. Harsoula, Celest. Mech. Dyn. Astr. **107**, 77 (2010).
[35] D. del-Castillo-Negrete, B. A. Carreras, and V. E. Lynch, Phys. Rev. Lett. **94**, 065003 (2005).
[36] M. Gerlach, S. Wüster, and J. M. Rost, J. Phys. B **45**, 235204 (2012).
[37] C. Zagoya, C. M. Goletz, F. Grossmann, and J. M. Rost, New J. Phys. **14**, 093050 (2012).